EPJ manuscript No.
(will be inserted by the editor)

F_2 challenging DGLAP

Dieter Haidt

DESY, D-22603 Hamburg, Notkestr. 85

Received: October 30, 2003

Abstract. The low-x data of the structure function F_2 measured by the collaborations H1 and ZEUS are compared with the prediction of the DGLAP equations. A new method of comparing data and theory is presented. The systematic and quantitative analysis shows that the predicted $1/x$ behaviour deviates increasingly from the observed one as x decreases below 10^{-3}.

PACS. 12.38.Bx QCD perturbative calculations – 12.38.Qk Experimental tests

1 Introduction

Lepton-nucleon experiments have paved the way towards the Standard Model with the observation of the proton substructure and the observation of weak neutral currents. Together with the ideas on gauge theories based on non-abelian algebrae and renormalizability a new framework for electroweak and strong interactions has been set up. A worldwide long term program was initiated.

Both the intermediate γ in e-nucleon and the intermediate W in ν-nucleon scattering probe the same internal structure of the nucleon. The Quark-Parton Model provided a simple interpretation of lepton-nucleon scattering, so for instance the structure function F_2 manifesting the fractional momentum distribution of quarks and antiquarks in the nucleon. The precise measurement of the momentum sumrule in the Gargamelle ν experiment [1] resulted in 0.50 ± 0.03 rather than 1. This surprising result indicated that quarks and antiquarks by far do not make up the momentum of the nucleon and another novel type of constituents, not visible to the W, must be present. They were attributed to the gluons as carriers of the strong force in the new microscopic theory of strong interactions QCD [2]. The apparently free behaviour of the partons observed in deep inelastic lepton nucleon scattering found its explanation in the property of the strong force to decrease at short distances. The immediate consequence was that the nucleon structure functions cannot be functions of the Bjorkén scaling variable x alone, but must depend on both kinematic variables characterizing deep inelastic scattering, namely x and Q^2, where Q^2 is the 4-momentum transfer squared from the lepton to the hadron system.

An impressive series of leptoproduction experiments of increasing precision was carried out. The differential cross section depends upon three structure functions F_2, F_L and xF_3. $\nu, \overline{\nu}$-experiments were distinguished by measuring in addition to F_2 also xF_3. The deep inelastic scattering experiments constituted a solid testing ground for QCD. In the kinematic regime, where Q^2 is sufficiently large, typically larger than 1 GeV^2, the strong interaction coupling constant $\alpha_s(Q^2)$ is small and a perturbative treatment is possible. The DGLAP evolution equations [3,4] offered an elegant way to test perturbative QCD in deep inelastic scattering experiments through the investigation of the deviation from scaling. Given the structure functions or the parton distribution functions as a function of x for a chosen starting value of Q^2_{st} QCD predicts the Q^2-evolution. The comparison between theory and experiment always involved a double aspect : the determination of the parton distribution functions, which cannot be predicted, and the properties of the theory to be tested.

The tests performed in the 70's and 80's were a great success and established the validity of the DGLAP equations in the $(Q^2, 1/x)$-phase space delimited to a triangular area by the size of the available beam energy, in practice reaching out in Q^2 to a few 100 GeV^2 and in x down to slightly below 10^{-2}. In comparing and interpreting the wealth of measurements there remained nevertheless a serious concern related to the arbitrariness in distinguishing the perturbative from the nonperturbative regime and to the correlations caused by the unknown gluon distribution function. As a matter of fact, the Q^2 evolution of the structure function xF_3 measured in $\nu, \overline{\nu}$ experiments tests QCD independently of assumptions about the gluon, however its statistical significance was much less than the precise F_2 measurements, which strongly depend upon assumptions about the gluon distribution function.

A new era of QCD tests started with the running of the ep-collider HERA 1992, which extended the phase space by two orders of magnitude in Q^2 and in x. The first data in the low-x region revealed a huge rise and thereby a new feature in the phenomenology of F_2. The subsequent detailed measurements by H1 [5] and ZEUS [6] offered new tests of QCD. They were performed by the experimental groups themselves as well as by various groups of theoretician. Recent global fits by MRST [7], CTEQ [8], GRV [9]

including the HERA data on F_2 resulted in good fits supporting thus the validity of the DGLAP evolution in the valence region up to Q^2 of order 10^4 GeV^2 and in the sea region, down to x=10^{-5}, up to the phase space limit. The successful extension of the fits up to the largest Q^2 values was expected. That the fits would still work at low-x was rather a surprise, as many were prepared to a failure of the perturbative approach, where terms with log $1/x$ should get numerically more and more prominent.

It is the purpose of this study to focus on the low-x regime of the $(Q^2, 1/x)$ phase space available in the HERA experiments, to investigate there in detail the rôle of the $1/x$ terms in the DGLAP kernels and to show that for x below 10^{-3} a discrepancy between theory and experiment develops.

1.1 Outline

Chapter 2 recalls some phenomenological aspects of F_2^{ep} reformulated in terms of a new variable q replacing ln Q^2. A new method of comparing data and theory is presented in chapter 3, which makes use of F_2, its first and second derivative in Q^2. The next chapter describes the decomposition of F_2^{ep} into a singlet and a nonsinglet part. Chapter 5 deals with the DGLAP equations formulated in terms of q and illustrates their effect when applied to a valence-like and a sea-like distribution separately for leading and next-to-leading order. After these preparations the main step is taken in chapter 6 with the evaluation of the curvature of the singlet part and F_2^{ep} itself. The last chapter concludes with the comparison of data and theory.

2 Phenomenology of F_2

The investigation of the Q^2 behaviour of the early low-x F_2 data measured by the HERA collaborations H1 and ZEUS suggested an approximate scaling behaviour [10,11] of the form $F_2 \sim \log Q^2/Q_0^2$ with $Q_0^2 \approx 0.5$ GeV^2. With the advent of further measurements extending to $Q^2 < 1$ GeV^2 it was desirable to have, instead of the usual ln Q^2, a quantity, which allows to examine the Q^2 dependence of the F_2 data in the neighborhood of 0. This is achieved[12] with the quantity [1]

$$q = \log(1 + \mathrm{Q}^2/\mathrm{Q}_0^2) \ , \qquad (1)$$

where Q_0^2 is a constant set to 0.5 GeV^2. The new quantity q is mathematically equivalent to the traditional ln Q^2, but has the feature to run from 0 to ∞. For $Q^2 \gg Q_0^2$ q is equivalent to ln Q^2, while otherwise it approaches Q^2. Fig. 1 illustrates the F_2-measurements by H1 [5] and ZEUS [6] as a function of q for a x-bin centered at x=10^{-4}. The structure function is within experimental uncertainties proportional to q over the full measured range corresponding to Q^2 from about 0.3 until 6.7 GeV^2, i.e. near to the HERA phase space limit. When the F_2 points are

[1] log is taken to base 10.

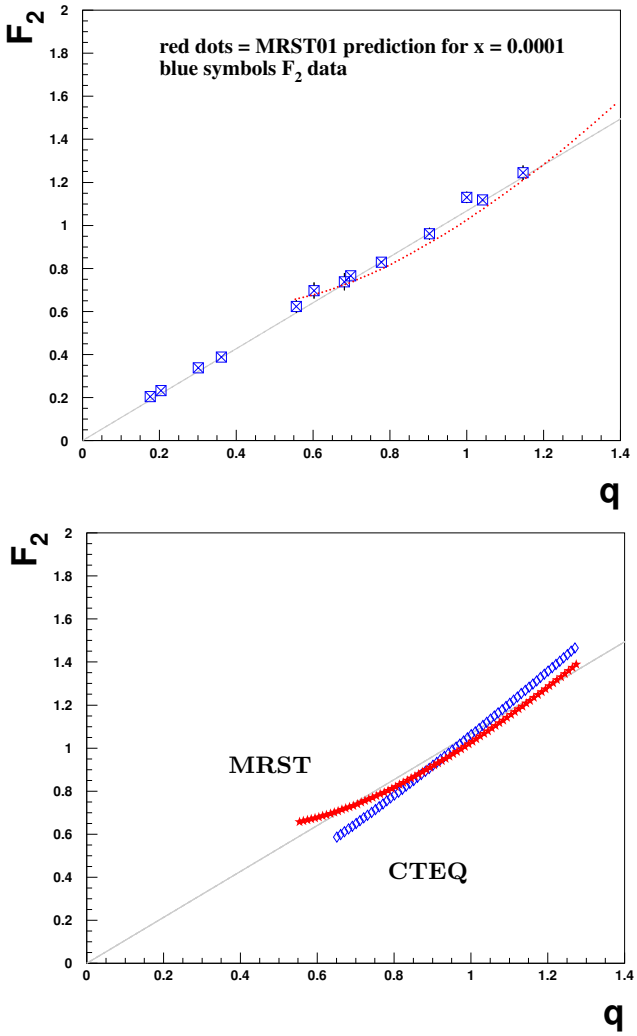

Fig. 1. The above figure shows the q-dependence of F_2-data for x-bin centered at x=10^{-4}; the dotted line is the prediction of the MRST01 parametrization. In the figure below predictions of the MRST01 and the CTEQ6 parametrization are compared for x=10^{-4}.

extrapolated towards Q^2=0 by a linear fit, a value for F_2 consistent with 0 comes out in agreement with the conservation of the electromagnetic current.

Fig. 1 shows also by the dotted line the prediction of the MRST parametrization[7] for x=10^{-4}, which is the result of their global fit. The fit is based on the x-dependence of the parton distributions a priori assumed at the starting scale Q_{st}^2 = 1.25 GeV^2, i.e. q_{st}=0.54, and then evolved in Q^2 using the DGLAP evolution equations (see eq. 4). The free parameters of the initial parton distributions are varied in an iterative procedure until the overall data and prediction yield a minimal χ^2. The comparison of the dotted line with the measured points illustrates that the global fit in this particular x-bin is a best fit, though not a good fit. In fact, there seems to be an indication for a difference in shape. This suggests the size of the second derivative

of F_2 w.r.t. q to serve as a test quantity in examining the validity of DGLAP in the deep sea.

The data of F_2 in the deep sea are well described by a second order polynom in q

$$F_2(x,q) = a_0(x) + a_1(x)\cdot q + a_2(x)\cdot q^2$$

where $a_0(x)$ and $a_2(x)$ are approximately 0, as seen for example in fig. 1. This form remains valid even in the valence region as long as q is restricted to the interval (0.5,2). The curvature term $a_2(x)$ is obtained as the second derivative of F_2 w.r.t. q, namely $\partial_q^2 F_2(x,q) = 2\,a_2(x)$.

The fig. 2 shows the curvature term $a_2(x)$ for the data at various fixed x-bins in comparison with the prediction of MRST. The lower limit in q is set to the starting scale for the DGLAP evolution in the MRST fit. The upper limit is chosen as small as possible such that there are still enough measurements to determine the curvature. This requirement led to $Q^2 < 12$ GeV^2 or $q < 1.4$, unless the HERA phase space limit is smaller. The experimental points are shown by the crosses, the MRST-points by the dots. The MRST-points are obtained applying the same procedure, but replacing the measured F_2 values by the corresponding values predicted by MRST. It should be noted that the average value of q decreases with decreasing x due to the more and more restricted phase space. The data are consistent with being flat in q, while the

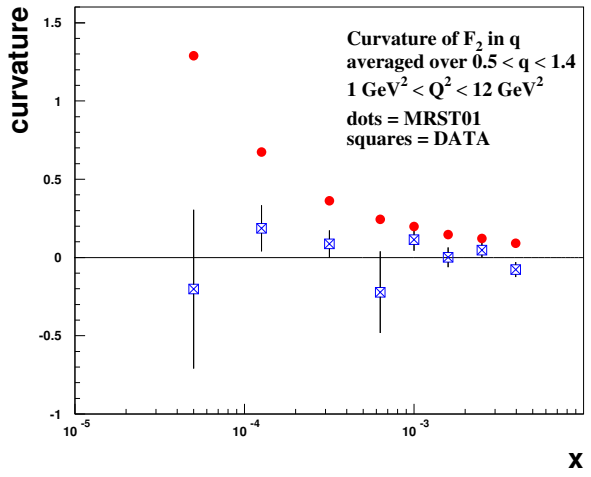

Fig. 2. Curvature of F_2 averaged over the interval $0.5 < q < 1.4$ for various fixed x-bins; the data points (squares) are compared with the MRST prediction.

MRST prediction deviates the more, the smaller x is.

3 Analysis method

The traditional way of testing the linear system of coupled DGLAP equations (see eq. 4) consists in performing the Q^2 evolution in form of a global fit, as indicated above (c.f. sect. 2). One single quantity, the overall χ^2, holds simultaneously the information on the shape of the parton distribution functions and on the validity of the DGLAP equations. A good fit means merely a consistency check for QCD.

A curve can be characterized in two distinct ways : either by points over a finite size or infinitesimally by one point and derivatives at this points. The method proposed here and elaborated relies on the latter characterization. Instead of performing the evolution of the singlet over the range in q, where measurements exist, the singlet is studied locally in q and the information about the q-behaviour is accounted for by considering the higher order derivatives w.r.t. q.

For all subsequent numerical calculations q is chosen to be 1 corresponding to Q^2=4.5 GeV^2. This value is big enough to justify the use of perturbative QCD and small enough to access the HERA F_2 measurements down to x=10^{-5} leaving two orders of magnitude in x for probing the low-x properties of the DGLAP kernels.

Given as input distributions the singlet $Q^+(x,1)$ and its derivative $\partial_q Q^+(x,1)$ the gluon distribution function $G(x,1)$ is derived from the first of the coupled DGLAP equations, as elaborated below in sect.6. In the next step the second derivative $\partial_q^2 Q^+(x,1)$ is calculated. There the unknown derivative $\partial_q G(x,1)$ emerges. The second of the coupled DGLAP equations provides precisely this term. The quantity $\partial_q^2 Q^+(x,1)$ is calculated in the deep sea and after relating it to $\partial_q^2 F_2(x,1)$ is compared with the experimentally determined curvature. This completes the local test of the validity of the DGLAP equations.

4 Decomposition of F_2^{ep}

The Q^2-evolution of the structure function F_2 in ep scattering proceeds differently for the singlet and the non-singlet part. The QCD expression for F_2^{ep} is given in terms of quark ($q_i(x,Q^2)$), antiquark ($\overline{q}_i(x,Q^2)$) density functions for each flavor i and the gluon function $g(x,Q^2)$:

$$F_2^{ep} = C_F \otimes N + \epsilon\ (C_F \otimes Q^+ + C_G \otimes G) \qquad (2)$$

This is the standard decomposition (see e.g. ref. [13]). The meaning of the variables is:

- Singlet : $Q^+ = \sum_i^f x(q_i + \overline{q}_i)$ with f the number of active flavors
- QED coupling constants : e_i^2 for flavor i.
- $\epsilon = \frac{1}{f}\sum_i^f e_i^2$
- Non-singlet : $N = \sum_i^f e_i^2 \left(x(q_i + \overline{q}_i) - \frac{1}{f} Q^+ \right)$
- Gluon : $G = xg$
- Coefficient functions C_F and C_G : C_F has a leading δ-function and a $\mathcal{O}(\alpha_s/2\pi)$ contribution, while C_G is directly of order to $\mathcal{O}(\alpha_s/2\pi)$.

The $\overline{MS}$ scheme is used and four massless quarks. F_2^{ep} is dominated by $N + \epsilon Q^+$, but receives subleading contributions from both the quarks and the gluon through the coefficient functions.

Detailed F_2^{ep} measurements are available from the two HERA collaborations H1 [5] and ZEUS [6]. The collaborations have provided in their publications careful analyses of systematic error sources. In their kinematic overlap region the data sets agree well, once the systematics is taken into account. Some of the correlated systematic sources affect not only the absolute values F_2, but also the derivative $\partial_q F_2$.

The structure function F_2^{ep} (eq. 2) is dominated by ϵQ^+ and receives contributions from the coefficient functions at $\mathcal{O}(\alpha_s/2\pi)$ and from the nonsinglet. For the actual calculations done below for q=1 it is then a good approximation to relate the x distributions of the singlet and its derivative to the well measured structure function as follows :

$$Q^+(x,1) = \frac{1}{\epsilon} F_2^{meas}(x,1)$$
$$\partial_q Q^+(x,1) = \frac{1}{\epsilon} \partial_q F_2^{meas}(x,1). \qquad (3)$$

In the kinematic region of interest, the deep sea with x <0.001, the non-singlet distribution contributes little to F_2 and $\partial_q F_2$. Furthermore, the convolutions of Q^+ and G with the coefficient functions only moderately modify the shape of the singlet distribution, both for the x and Q^2 dependences. The small corrections implied by the identification given in eq. 3 are considered in sect.7.

5 The DGLAP equations

From the parton density functions of the quarks $q_f(x,Q^2)$, antiquarks $\overline{q}_f(x,Q^2)$ for the active flavors f and the gluon $g(x,Q^2)$ one can form the following distributions :

$$\begin{array}{lll} Valence & Q^- & = \sum x(q_i - \overline{q}_i) \\ Singlet & Q^+ & = \sum x(q_i + \overline{q}_i) \\ Gluon & G & = xg. \end{array}$$

For the values of Q^2 considered f=4 is assumed and furthermore all quarks are taken to be massless.

The DGLAP integro-differential equations for the singlet and the gluon read in compact form :

$$\partial_q \begin{pmatrix} Q^+ \\ G \end{pmatrix} = a(q) \begin{pmatrix} P_{qq} & P_{qg} \\ P_{gq} & P_{gg} \end{pmatrix} \otimes \begin{pmatrix} Q^+ \\ G \end{pmatrix} \qquad (4)$$

The equations are formulated in terms of the variable q rather than the usual ln Q^2. The variable transformation ln $Q^2 \rightarrow q = \log(1 + Q^2/Q_0^2)$ implies

$$\mathrm{d}\, q = \frac{Q^2}{Q^2 + Q_0^2} \frac{1}{\ln 10}\, \mathrm{d}\ln Q^2,$$

where the Jacobi factor $Q^2/(Q^2 + Q_0^2)$ appears and the factor ln 10, since the variable q is defined with log to base 10. The notation ∂_q is a shorthand for $\partial/\partial q$. Furthermore,

$$a(q) = \frac{\alpha_s(Q^2)}{2\pi} \frac{Q^2 + Q_0^2}{Q^2} \ln 10.$$

It is interesting to note, that $q \cdot a(q)$ has only a small Q^2-dependence: it increases by 3 % in going from 5 to 50 GeV^2 and decreases by 3 % in going from 5 to 1 GeV^2.

The kernels P_{ij} describe the splitting of parton $j \rightarrow i$. They are used in next-to-leading order in the $\overline{MS}$-scheme as published in ref. [13] :

$$P(x,\alpha_s) = P^{LO}(x) + \frac{\alpha_s}{2\pi} P^{NLO}(x).$$

The leading and next-to-leading kernels are by themselves functions of x alone. However, the full kernels receive a Q^2 dependence indirectly through the Q^2 dependence of the QCD coupling α_s.

A characteristic feature of all four kernels consists in the fact that they contain in next-to-leading order terms proportional to $1/x$, the two kernels P_{qg} and P_{gg} even already at lowest order. Their presence provokes an almost explosive rise at values of $x < 0.001$, as illustrated in fig. 3 for the off-diagonal kernels P_{qg} and P_{gq}. Their behavior becomes singular for $x \rightarrow 1$ and is not shown. In the deep

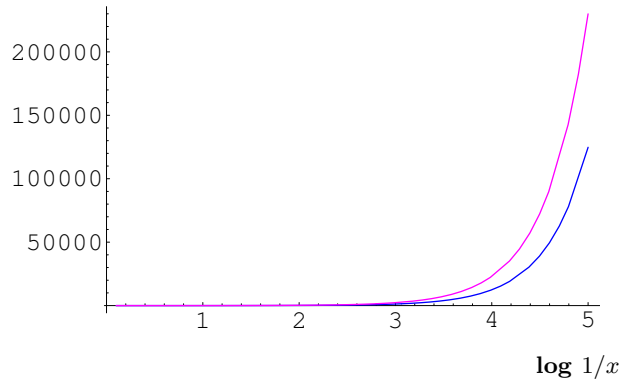

Fig. 3. The kernels P_{qg} and P_{gq} vs. log $1/x$; the upper curve refers to P_{gq}. The log $1/x$ starts at 0.1 excluding the singular behaviour of x near to 1.

sea region the x behaviour of P_{qg} and P_{gq} is similar, this leads in their ratio to a nearly x independent shape, as displayed in fig. 4. The two diagonal kernels P_{qq} and P_{gg}

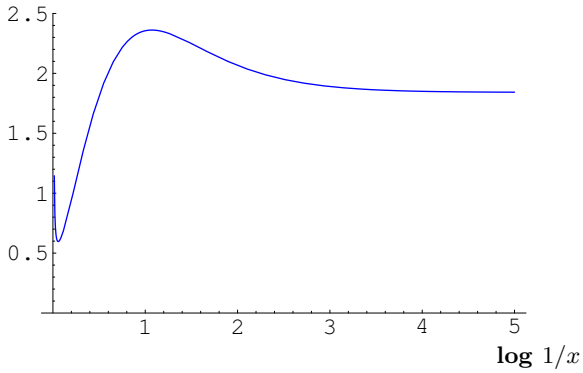

Fig. 4. The ratio P_{qg}/P_{gq} for 0.00001 < x < 0.97.

include *distributions*, i.e. *plus*- and δ-functions, and cannot be displayed directly. Instead, the properties of a kernel P can be studied by comparing a given distribution function f with the corresponding folded distribution function $P \otimes f$:

$$f(x) \rightarrow P \otimes f(x).$$

The convolution of a function $f(x)$ with the kernel $P(x)$ is defined by :

$$P \otimes f(x) = \int_x^1 \mathrm{d}\xi \, P(\xi) \, f(\frac{x}{\xi}).$$

The integral runs from x to 1, consequently the value of the folded distribution at $\hat{x}$ involves the functional dependence of the input function from $\hat{x}$ until 1. The graphical representation of the x dependence is conveniently given in terms of $\log 1/x$.

For illustration the convolution effect is demonstrated for two adhoc, but typical functions, a *valence* like distribution (f_{val}) and *sea* like distribution (f_{sea}).

5.1 Study of $f_{val}(x) \rightarrow a(q) \; P(x, \alpha_s(q)) \otimes \; f_{val}(x)$

Fig. 5 shows on top the *valence* like distribution :

$$f_{val}(x) = 3.28 \; \sqrt{x}(1-x)^3$$

and below (b and c) for q=1 the distributions resulting from the folding with the four kernels. The factor 3.28 is chosen to make the integral over the corresponding density equal to 3. The diagonal kernels generate the characteristic shape, which causes the depletion of the input distribution in the valence region and the corresponding gain in the sea region. There is a marked difference between P_{qq} and P_{qg} at lowest order and full order in the sea region. It originates from the fact, that in the leading order kernels $1/x$ terms are absent, while present at next-to-leading order. On the contrary, the other two kernels, P_{gq} and P_{gg}, have $1/x$ terms both at leading order and next-to-leading order and the leading order contribution dominates. The above mentioned divergences of the kernels P_{gq} and P_{gg} for $x \rightarrow 1$ are absent in $P \otimes f_{val}$ due to the power behaviour of f_{val} near to 1.

The convolution of a valence like function leads in the deep sea to a flat shape for all four kernels, as expected for $1/x \; \otimes \; f_{val} \rightarrow \; constant$. The plateau heights are characteristically different : smallest for P_{qq} and largest for P_{gg}.

5.2 Study of $f_{sea}(x) \rightarrow a(q) \; P(x, \alpha_s(q)) \otimes \; f_{sea}(x)$

Similarly, fig. 6 shows the four convolutions of a *sea* like distribution function chosen to be

$$f_{sea}(x) = 1.5 \; \log\left(1 + \frac{0.04(1-x)}{x}\right).$$

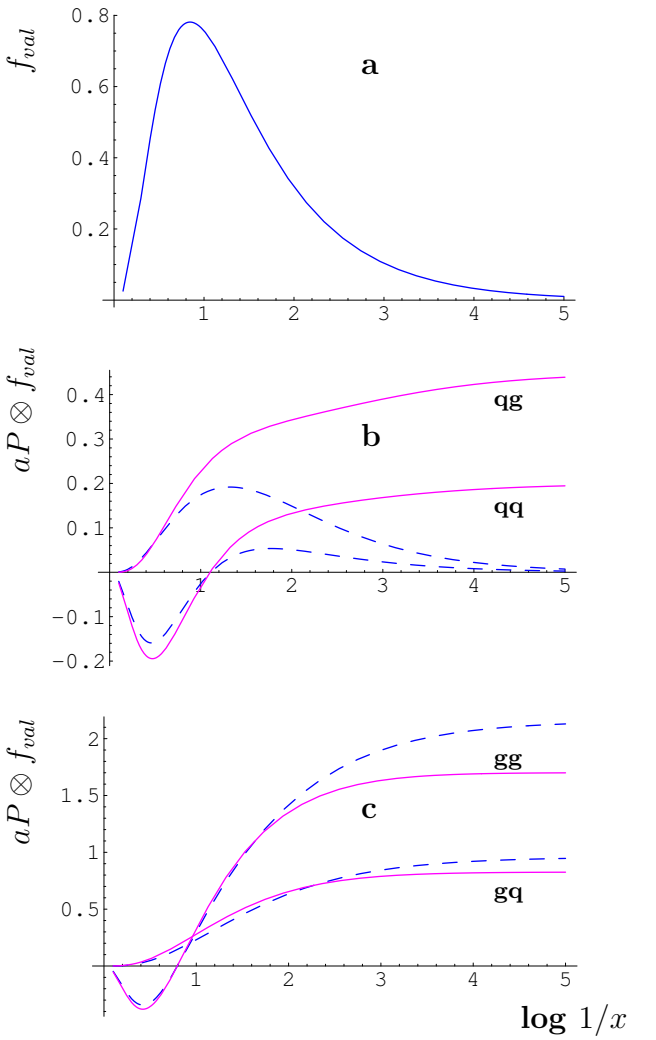

Fig. 5. a. The valence-like distribution $f_{val}(x)$ versus log $1/x$. **b.** $a(q) \; P_{qq} \otimes f_{val}$ and $a(q)P_{qg} \otimes f_{val}$ for q=1 versus log $1/x$. **c.** $a(q)P_{gg} \otimes f_{val}$ and $a(q)P_{gq} \otimes f_{val}$ for q=1 versus log $1/x$. The solid (dashed) curves show the convolution with the full (leading) order kernel marked with the appropriate indices. The curves resulting from the folding with the diagonal kernels P_{qq} and P_{gg} show the characteristic underswinger in the valence region.

It is similar to Q^+ with regard to the behaviour in the deep sea (see fig. 7a). The asymptotic behaviour in the deep sea is again determined by the $1/x$ terms of the kernels with the effect that the linear logarithmic behaviour turns into a quadratic one. The properties of the kernels generate a pattern analogous to the *valence* like case. The $P_{qq} \otimes \; f_{sea}$ becomes very small, while $P_{gg} \otimes \; f_{sea}$ is strongly enhanced in the deep sea.

5.3 Some conclusions

The two opposite cases may serve to estimate the effect of a modification in the input distributions regarding the

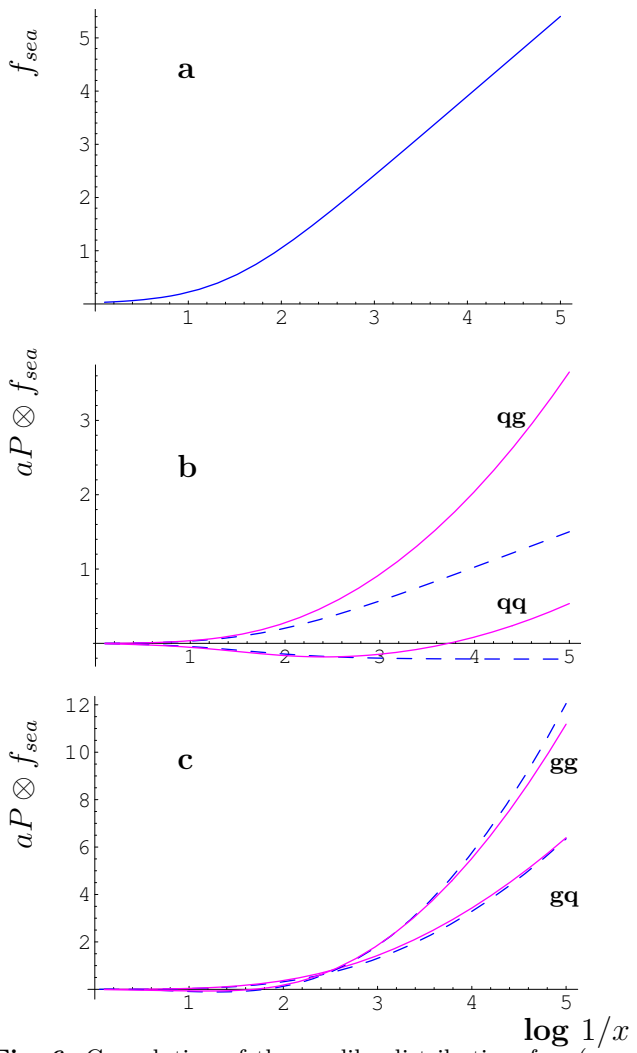

Fig. 6. Convolution of the sea-like distribution f_{sea} (uppermost curve) with the four kernels P_{ij} vs. log $1/x$. Explanation of the curves as in caption of fig. 5 exchanging *val* by *sea*.

size and shape of the folded distributions. Three simple examples may illustrate it : (a) Adding to the gluon function a small *valence* like contribution would affect $\partial_q Q^+$, the slope of the singlet, in the deep sea by a small x-independent upward shift. Fig. 5b allows for a quantitative evaluation. (b) Consider fig. 1. Suppose a small *sea* like contribution is added to the shape of the gluon distribution function, then fig. 6b shows that to $\partial_q Q^+$ in the deep sea would be added a term quadratic in log $1/x$, thus generating a nontrivial increase of the curvature of the singlet Q^+. (c) It is also clear, that a small modification of the x-dependence of the singlet Q^+ (for given q) does not sizeably affect its slope in q.

It is interesting to note that all folded distributions are positive in the deep sea region regardless whether they are *valence* or *sea* like. This is different in the valence region. Therefore, compensating effects in the coupled DGLAP are possible in the valence region, but not so in the deep sea region.

Even if the distribution function f is independent of q, the folded distribution function $P_{ij} \otimes f$ depends upon q through the α_s dependence of the kernels P_{ij}.

6 The Curvature

The 1^{st} of the coupled DGLAP equations (see eq. 4), i.e.

$$\partial_q Q^+ = a(q)\left(P_{qq} \otimes Q^+ + P_{qg} \otimes G\right) \tag{5}$$

is differentiated w.r.t. q in order to obtain the required test quantity, yielding

$$\partial_q^2 Q^+(x,q) = (Quark-term) + (Gluon-term). \tag{6}$$

Each of the two terms consists in turn of three contributions.

The *Quark-term* is numerically small, because the q-dependences of Q^+ and of $a(q)$ nearly compensate each other, as mentioned in sect.3. The numerical result is shown in fig. 8 by curve d.

The *Gluon-term* with its three contributions is given explicitly in the following equation 7 :

$$\begin{aligned}\partial_q\Big(a(q)P_{qg} \otimes G(x,q)\Big) = \\ + \ (\tfrac{a'}{a} + \tfrac{\alpha_s'}{\alpha_s}) \cdot a(q)\ P_{qg} \otimes G \\ - \ \tfrac{\alpha_s'}{\alpha_s} \cdot \quad a(q)\ P_{qg}^{LO} \otimes G \\ + \quad\quad a(q)\ P_{qg} \otimes \partial_q G\end{aligned} \tag{7}$$

The prime ($'$) in eq. 7 denotes the derivative w.r.t. q. Eq. 7 involves both the gluon distribution function G and its derivative $\partial_q G$. A closer inspection of the formula shows, however, that the dependence on the gluon is not strong. To this end it is noted that the expression $a(q)\, P_{qg} \otimes G$ follows directly from the 1^{st} DGLAP equation (eq. 5), namely

$$a(q)\, P_{qg} \otimes G = \partial_q Q^+ - a(q)\, P_{qq} \otimes Q^+. \tag{8}$$

It is determined by the experimental input distributions $Q^+(x,1)$ (see curve a in fig. 7) and $\partial_q Q^+(x,1)$. The gluon distribution function $G(x,1)$ itself can be obtained from the constraint equation 8. Given the properties of the kernel P_{qg} the magnitude and shape of $G(x,1)$ are defined and little scope for variations is left. Fig. 7 (curve c) shows the resulting distribution.

The three terms of eq. 7 are discussed one by one and evaluated for q=1.

- **Term 1:** The x dependence is given by eq. 8, since the factor $a'/a + \alpha_s'/\alpha_s$ is independent of x and, for q=1, equals to -1.3.
- **Term 2** involves the gluon folded with the leading order kernel P_{qg}^{LO}, which has the simple form $x^2 + (1-x)^2$; it is numerically insignificant.
- **Term 3** involves $\partial_q G$ and is the critical one. The expression for $\partial_q G$ is given by the 2^{nd} of the coupled DGLAP equations (eq. 4)

$$\partial_q G = a(q)\left(P_{gq} \otimes Q^+ + P_{gg} \otimes G\right). \tag{9}$$

Insertion in term 3 yields :

$$a(q)\, P_{qg} \otimes \partial_q G = a(q)\, P_{qg} \otimes G \cdot a(q)\, \frac{P_{qg} \otimes (P_{gq} \otimes Q^+ + P_{gg} \otimes G)}{P_{qg} \otimes G}$$

The first factor (eq. 8) does not depend upon the gluon, while in the second factor, the ratio, the gluon appears both in the numerator and the denominator. Its magnitude cancels and its shape affects the ratio only weakly. In the deep sea the ratio is well approximated by

$$1.2\; a\; \frac{P_{qg} \otimes P_{gg}^{LO} \otimes G}{P_{qg} \otimes G}.$$

Recalling the structure of the kernels it is quite evident that the numerator is sensitive to $\frac{1}{x} \otimes \frac{1}{x}$, while the denominator only to one $\frac{1}{x}$-operator. It is then not so surprising that term 3 with $\partial_q G$ dominates the behaviour in the deep sea and produces unavoidably a strong x-dependence.

The quantitative evaluation of the contributions to the curvature is carried out using the singlet and gluon distribution functions displayed in fig. 7. The results are shown

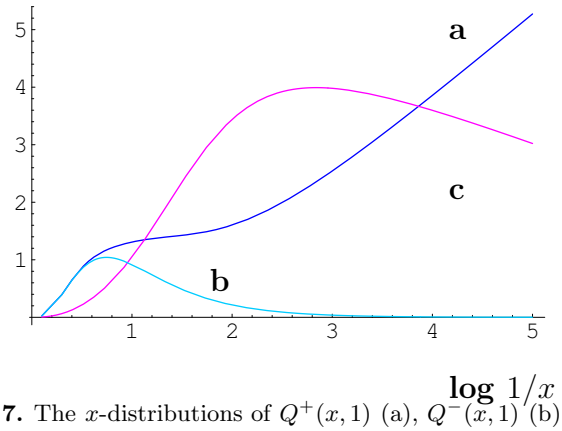

Fig. 7. The x-distributions of $Q^+(x,1)$ (a), $Q^-(x,1)$ (b) and the gluon $G(x,1)$ (c).

in fig. 8. The contribution of the *Quark-term* (curve d) is negative and very near to 0, as anticipated. The three contributions from the *Gluon-term* decrease linearly (a), remain approximately constant (b) and increase quadratically (c).

It is concluded that $Q^+(x,q)$ has a significant positive curvature in the deep sea region, where the contribution from $\partial_q G$ outnumbers all other contributions. The x behaviour of the curvature is a *property of the kernels* and is hardly sensitive to the size and shape of the gluon. The quantity $\partial_q^2 Q^+(x,q)$ probes in a nontrivial way both DGLAP equations and their kernels.

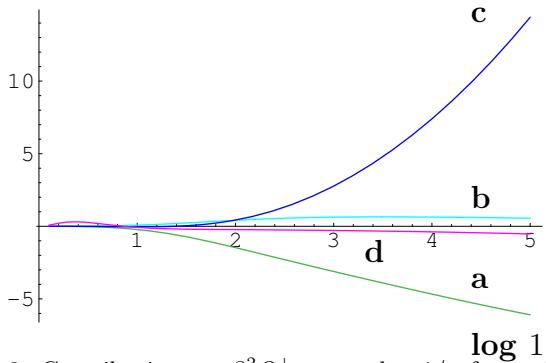

Fig. 8. Contributions to $\partial_q^2 Q^+$ versus log $1/x$ for q=1. The curves represent the *Quark-term* (d) and the three contributions of the *Gluon-term*, i.e. term 1 (a), term 2 (b) and term 3 (c).

7 Prediction of $\partial_q^2 F_2^{ep}$

The theoretical expression for F_2^{ep} is given in eq. 2. It involves the parton distributions and the coefficient functions C_F and C_G. The quantity to be determine is the second derivative of F_2^{ep} w.r.t. q, i.e.

$$\partial_q^2 F_2^{ep} = \partial_q^2 \Big(C_F \otimes (N + \epsilon\; Q^+) + C_G \otimes \epsilon G \Big)$$

evaluated in the deep sea and for $q = 1$. In addition to the dominating contribution of $\partial_q^2 Q^+$ discussed in sect.6 also the effect of the non-singlet N and the coefficient functions together with their respective derivatives have to be considered.

C_F, the first coefficient function, consists of two distributions, a δ-distribution, which reproduces $N + \epsilon\; Q^+$ and a *plus*-distribution applied to $N + \epsilon\; Q^+$ contributing at order $\alpha_s/2\pi$.

$N + \epsilon\; Q^+$ is dominated by the singlet Q^+. Even in the deep sea the non-singlet N is not vanishing, since at $Q^2 = 4.5$ GeV^2 the charmed sea is not yet fully developped implying $\overline{c} - \overline{s} < 0$. However, the evolution of the non-singlet contributes negligibly to the first and second derivative of F_2^{ep}.

The gluon and its derivatives w.r.t. q contribute directly through the second coefficient function C_G and also in the evaluation of $\partial_q^2 Q^+$.

The figure 9 shows the contribution arising from the coefficient functions to $N + \epsilon Q^+$ and its derivatives. As anticipated, $N + \epsilon Q^+$ is a good approximation to F_2^{ep} and as well for the first derivative w.r.t. q. The second derivative is modified in the deep sea regime by less than about 10 %. The contribution of the non-singlet to $\partial_q^2 F_2$ is negligible.

In conclusion : The statement, that $\partial^2 Q^+$ is significantly positive, remains valid also for $\partial^2 F_2^{ep}$. This conclusion is stable against variations of the input distributions.

It may be noted that, qualitatively, the feature of a positive curvature can be deduced already from the theoretical study [14] predicting an unbounded growth of F_2 with $1/x$ under certain uniformity assumptions.

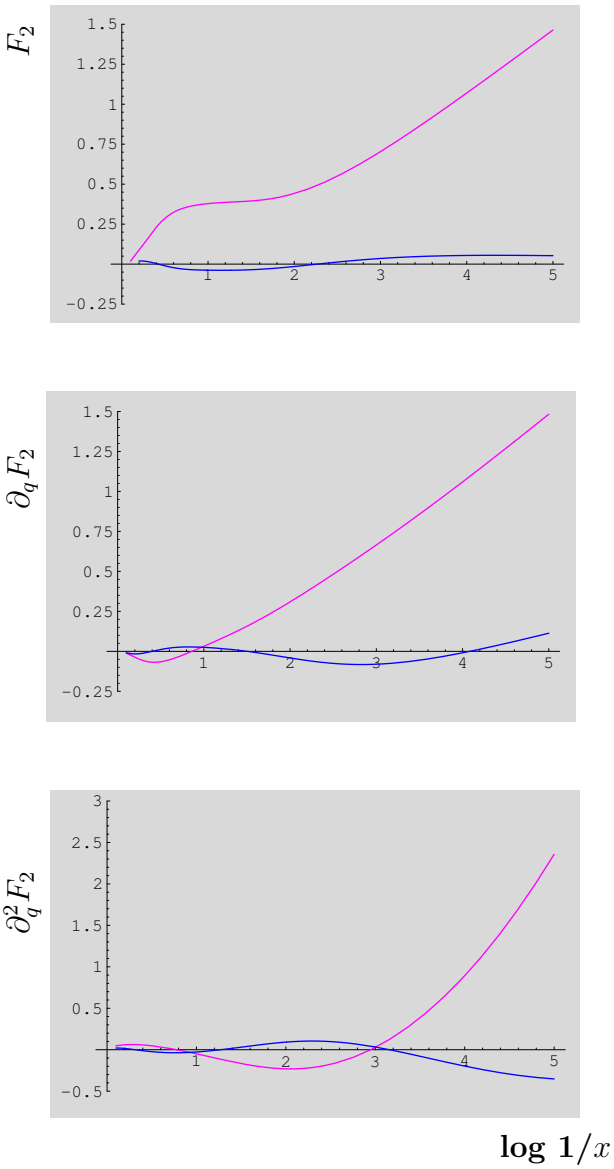

Fig. 9. Effect of the coefficient functions to $N + \epsilon Q^+$ and its derivatives versus log $1/x$ for q=1.

8 Conclusions

A dedicated investigation of the DGLAP kernels in the low-x regime has been performed. Their striking feature is the presence of $1/x$ terms producing a strong rise in F_2 for x <0.001. Previous QCD analyses based on low energy lepton-nucleon data did not probe that behaviour, since they reached in x hardly below 0.01. Recent global QCD analyses, which also include the low-x HERA F_2 data, are only partially sensitive to the low-x behaviour of the kernels, because the relevant data represent a small fraction of the data entering the global fit und thus their effect to the overall χ^2 remained unnoticed.

The study presented here was focussed directly on the deep sea and has examined the second derivative of the structure function F_2^{ep} w.r.t. q as a quantity for probing the low-x feature of the DGLAP kernels. The main result is shown in fig. 10. The DGLAP kernels predict a significant positive curvature of F_2 at fixed q=1 in the low-x region in contrast to the flat behaviour in q of the HERA F_2-data. This conclusion is stable against changes of the shape of the parton distribution functions, in particular of the gluon distribution.

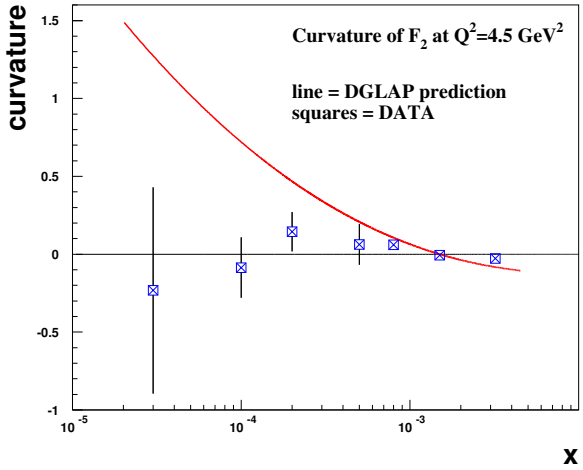

Fig. 10. Measured and calculated curvature of F_2 for q=1 versus x.

It is interesting to note that $P_{ij} \otimes f$ is positive for all kernels provided x is deep enough in the sea region and f positive definite. This implies for the DGLAP equations that in the deep sea the derivatives of the singlet and the gluon receive positive contributions from both the folded singlet and the folded gluon, contrary to mutual compensations possible in the valence region.

Acknowledgement

I like to thank J. Bartels, T. Gehrmann, H. Spiesberger and P.M. Zerwas for valuable discussions.

References

1. T. Eichten et al., Phys.Lett. **B46** (1973) 274-280
2. P.M. Zerwas and H.A. Kastrup, **QCD - 20 years later**, World Scientific, Singapore 1993, 1-867
3. V.N. Gribov, L.N. Lipatov, Yad.Fiz.**15** (1972) 781-807, Sov.J.Nucl.Phys.**15** (1972) 438-450
4. G. Altarelli, G. Parisi, Nucl.Phys.**B126** (1977) 298
5. C. Adloff et al.: Nucl.Phys.**B497** (1997) 3-30
   S. Aid et al.: Nucl.Phys.**B470** (1996) 3-40
   T. Ahmed et al.: Nucl.Phys.**B439** (1995) 471-502
   C. Adloff et al.: Eur.Phys.J.**C30** (2003)1

6. J. Breitweg et al.: Phys.Lett.**B487** (2000) 53; (BPT)
J. Breitweg et al.: Phys.Lett.**B407** (1997) 432; (BPC)
M. Derrick et al.: Z.Phys.**C69** (1996) 607;
J. Breitweg et al.: Eur.Phys.J.**C7** (1999) 609; (SVX)
S. Chekanov et al.: Eur.Phys.J.**C21** (2001) 443;
7. A.D. Martin et al., Eur.Phys.J **C23** (2002) 73.
8. J. Pumplin et al., hep-ph/0201195 (2002).
9. M. Glück, E. Reya, A. Vogt: Eur.Phys.J.**C5** (1998)461-470
10. D. Haidt, *DIS96*, Rome, April 1996, World Scientific Publishing, 1997, 179.
11. W. Buchmüller and D. Haidt, Double Logarithmic Scaling of the Structure Function F_2 at Small x, hep-ph/9605428
12. D. Haidt, *DIS97*, Chicago, April 1997, AIP Conference Proceedings 407 (1997) 386.
13. W. Furmanski and R. Petronzio, Z.Phys. **C11** (1982) 293-314.
14. A.De Rujula et al.: Phys.Rev. D **10** 1974, 1649.